The Light Production of the MINOS Mini Calibration Module

Christopher Smith

13th June 2000

First Year Report

Abstract

MINOS is a long baseline experiment planning to start searching for evidence of neutrino oscillations in late 2003. The experiment consists of two detectors and intends to compare the results obtained from both in order to make measurements. The need to compare the two detectors in this way brings forth the need for calibration.

The MINOS mini calibration module, constructed at UCL, is designed to be similar to the real MINOS detectors in all important aspects. The intention of this report is to provide a preliminary calculation of the light yield of the module by considering the passage of muons through the detector. This was acheived by putting the module in a PS test beam at CERN.

University College London

1 Introduction

The Standard Model of Particle Physics (SM) predicts that all matter is composed from six quarks, six leptons (three charged and three neutral), and their antiparticles. It further states that all interactions between them can be explained by the exchange of one of a number of gauge bosons. Many experiments have been designed and performed to test the validity of the model, and, so far, it has proven to be very successful. However, it is expected (and hoped) that there is physics beyond the SM and one promising field in which investigations are underway is that of neutrino physics.

In the SM, there are three neutrino flavours, corresponding to the three charged leptons, the electron, muon and tau. The neutrinos are massless, carry no electromagnetic or strong charge and therefore, can only interact via the weak interaction. These properties mean that neutrinos very rarely leave any trace of their passage through matter, making their detection very difficult. This in turn makes the determination of the true nature of the neutrino more complicated.

The belief that the SM does not completely or accurately describe neutrinos is motivated by a number of independant facts. It is known that flavour mixing is observed for hadrons. The weak eigenstates for quarks are not the same as the mass eigenstates, thus allowing quarks to apparently transmute to other quarks in weak interactions. The probabilities for such interactions are given by the Cabbibo-Kobayashi-Maskawa (CKM) mixing matrix. From a theoretical point of view, it is conceivable that leptons have a similar freedom which would give rise to a mixing matrix for neutrinos.

Experimentally, there is evidence for a disagreement between the predicted and measured numbers of neutrinos arriving at the Earths surface. The Super-Kamiokande experiment uses a high-mass (50 kiloton) water Cerenkov detector to identify the charged leptons produced when a ν_μ or ν_e interacts in its fiducial volume. Detectors such as this are being used to investigate two isolated problems: The Solar neutrino problem highlights the apparent dirth of ν_e arriving from the sun compared to the number predicted by the Solar Model, (ν_μ cannot be measured as they are not energetic enough to produce μ's in the detector).

The Atmospheric neutrino problem addresses the ratio of the number of ν_μ to ν_e reaching the Earths surface from the upper atmosphere as a result of Cosmic Ray collisions with nuclei. The theoretical ratio for this is 2:1 in favour of ν_μ , however, the experiments fail to measure this.

Over a number of years, this evidence has led to a possible explanation, first suggested by Pontecorvo [1] in 1967; namely, neutrino oscillations. If it is postulated that neutrinos have a finite mass, and that, like for quarks, the weak and mass eigenstates are not the same, then any neutrino produced in an interaction contains a mixture of all three mass eigenstates. Since neutrinos have no equivalent to hadronisation in quarks, they will continue to be a mixture until they interact again. Moreover, the probability of a particular mixture will depend on a number of variables as shown in the formula below.

$$P_{\alpha\beta} = \mid \delta_{\alpha\beta} - sin^2 2\theta sin^2(1.27\Delta m^2 L/E_\nu) \mid$$

This formula gives the oscillation probability for two generation neutrino mixing, where $P_{\alpha\beta}$ is the probability that there is an oscillation between flavours α and β; θ is the mixing angle; $\Delta\mathrm{m}^2$ is the mass difference squared between the two mass eigenstates in units of eV^2/c^2; L is the neutrino path length in km and E_ν is the neutrino energy in GeV. When the formula is extended for three generations, the mixing angle term is modified but the dependance on L, $\Delta\mathrm{m}^2$ and E_ν remains the same.

With such a formula, one may expect that experiments like Super-Kamiokande could directly compare their findings with predictions from atmospheric and solar neutrino physics allowing for oscillations. However, this is not the case since these experiments have no control over the energy of neutrinos they receive and so the detection of a signal for neutrino oscillation involves a complicated analysis of the data.

A different approach to the neutrino problem is taken by the so-called long-baseline experiments. An example of this type of experiment is the MINOS experiment, in which a neutrino beam is produced at the Main Injector at Fermilab near Chicago and is fired approximately 730km through the Earth towards a detector in Minnesota. Figure 1 shows a schematic diagram of the experiment. A near detector is also installed to intercept and measure the beam before any oscillations have occured.

In such an experiment, the detectors must be very large to ensure a high enough event rate, which means that the baseline (the distance L in the oscillation formula) is fixed before the experiment even begins. $\Delta\mathrm{m}^2$ is fixed by nature herself which leaves only the energy of the neutrinos available for adjustment. This is where the power of MINOS lies. By knowing the energy of the neutrinos and how far they have travelled, accurate limits can be put on the values of $\Delta\mathrm{m}^2$ and $\sin^2 2\theta$. The MINOS experiment will work at low beam energies in order to maximise its sensitivity to low $\Delta\mathrm{m}^2$. This allows the region of neutrino oscillation parameter space suggested by atmospheric neutrino physics to be explored ($\sin^2 2\theta \sim 1$ and $\Delta\mathrm{m}^2 > 10^{-3} eV^2$).

2 The MINOS Experiment

2.1 Physics Capabilities

The physics capabilities of the MINOS experiment allows for three groups of potential measurements: statistical measurements, $\nu_\mu \rightarrow \nu_e$ identification and study

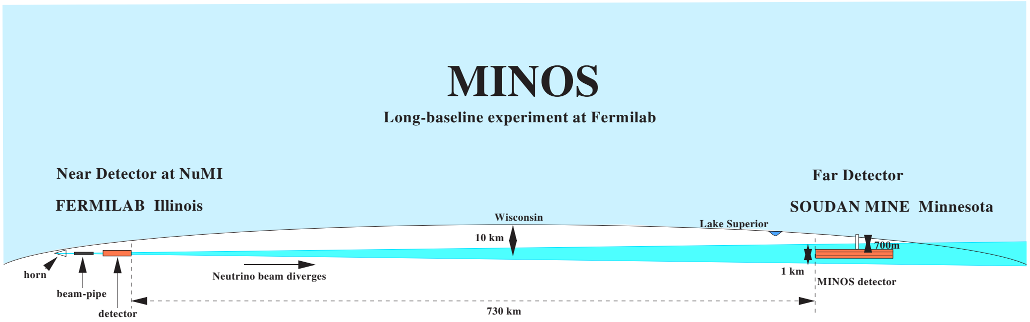

Figure 1: The MINOS experiment.

of exclusive τ decay channels. All these measurements are sensitive to neutrino oscilations and are complementary.

The statistical measurements essentially involve looking at four independant quantities: The rates and energy spectra for both neutral current (NC) and charged current (CC) interactions. From the CC rates and energy spectra, any mode of oscillation can be detected by the depletion of ν_μ events and a comparison of the near and far energy spectra will provide information about $\sin^2 2\theta$ and Δm^2.

The ratio of ratios $(NC/CC)_{near}/(NC/CC)_{far}$ is also a very useful measurement for two reasons. Firstly, it eliminates problems due to differing rates at the near and far detector since, any systematic errors are cancelled in the ratios; and secondly, it is sensitive to oscillations not only because of the falling number of CC events but also because most of the ν_τ and all of the ν_e will interact via NC channels.

The long term plans for the MINOS experiment have not yet been decided. Depending on the initial run results, upgrades to the experiment may be considered or different beam specifications may be selected. For example, an emulsion-based upgrade may be implemented should $\nu_\mu \to \nu_\tau$ oscillations be discovered [2; chapter 3].

2.2 The Beam

The NuMI (Neutrinos at the Main Injector) neutrino beam will be the most intense source of neutrinos in the world and is the reason that we can undertake this type of experiment. The neutrino beam will contain predominantly ν_μ resulting from the decay of π's and K's produced when protons from the main injector are brought to focus on a carbon target. Magnetic horns, which perform the focusing, allow a neutrino beam with one of three different energy spectra to be produced. When the beam is first switched on, the lowest energy beam will probably be used; the ν_μ component of the beam will peak at approximately 4 GeV at the far detector.

This allows sensitivity to $\nu_\mu \rightarrow \nu_\tau$ oscillations via the observation of tau leptons (tau production threshold $\approx$ 3.5GeV).

2.3 The Far Detector

The MINOS far detector will be built within a caveren in the Soudan mine, North Minnesota, at a depth of 2100 metres of water equivalent (m.w.e). Everything required for the construction, including the detector components and machinery, will be transported down a small mine shaft in parts and reassembled underground.

The detector is a large tracking iron calorimeter and is made up from a series of modules. Each module consists of an inch thick, octagonal, planar steel sheet followed by an active element of solid scintillator. Modules are 8 metres wide each and 484 of these will comprise the far detector. The detector is split up into 2 supermodules each with 243 steel planes. Each supermodule is independantly fitted with a 15kA-turn coil to provide a magnetic field in the iron of, on average, 1.5 Tesla. Figure 2 is a schematic diagram of the far detector.

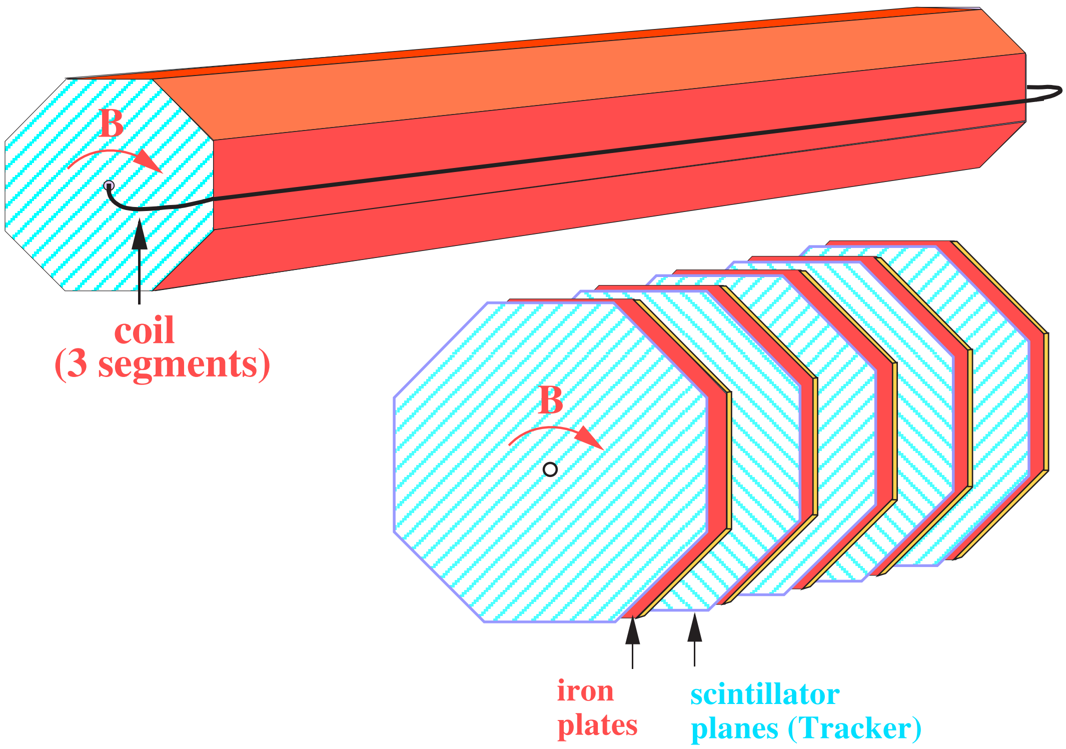

Figure 2: The far detector modules

Each scintillator plane will be constructed from 192 strips with cross-section 4.1 x 1.0 cm. The length of each strip will depend on its position in the plane. The orientation of the scintillator strips alternates by $\pm 90^o$ in successive planes. Readout from each strip will be acheived by embedding a wavelength shifting fibre (WLS) along its length to capture, wavelength shift and transport light to the two ends. The WLS is then coupled to clear optical fibre at both ends and the light is transported to multipixel photomultiplier tubes.

2.4 The Near Detector

The near detector is required as a reference for the far detector. It will be used to obtain a direct measurement of the beam before oscillations have occured. This therefore reduces the dependance of the experiment on Monte Carlo calculations and the measurements can be compared to equivalent measurements at the far detector to see if oscillations have occured.

To ensure an unbiased comparison, the beam, detectors and experimental environment must be as similar as possible at both locations. Flux differences in the neutrino beam at the different locations is an unavoidable consequence, but can be accounted for, as can differences in neutrino energy spectrum due to the decay kinematics of the original π's and K's.

The near detector is as close to the far detector in design as possible in all important features. The absorber planes and active layers are identical in nature and measure the same in relevant dimensions. Also, the strength of the magnetic field is the same. The shape is that of an elongated octagon, 3.8 metres high and 4.8 metres wide. The neutrino beam will be directed at a point offset from the centre of the detector, thus reducing the amount of steel used and the amount of scintillator and instrumentation needed.

Figure 3 is a schematic diagram of the near detector, showing the instrumented regions.

3 Calibration

3.1 The Need for Calibration

An important area of research, currently being worked on at UCL, among other institutions, is that of calibration. Without a full understanding of all aspects of both detectors, the power gained from the ability to compare the near and far measurements, is lost because of ambiguity in the relationship between the outputs of each detector.

Although, the initial measurements of, for example, $(NC/CC)_{near}/(NC/CC)_{far}$ are independant of the beam to first order, it will be necessary to make a cut on the energy of NC events to be included in the ratio (since for low energy neutrino scattering, it becomes difficult to make accurate measurements). Calibration is vital

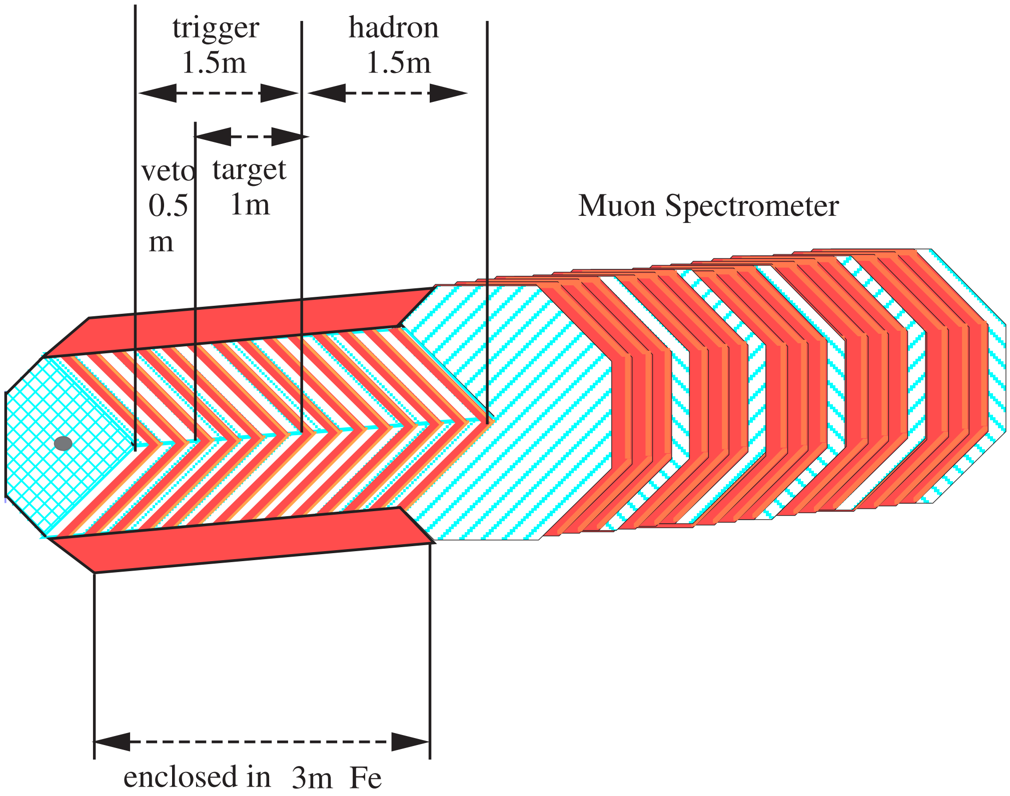

Figure 3: The instrumented regions of the near detector.

therefore, in order for a direct comparison of the ratios at the near and far detector to be valid.

Also, subsequent measurements of the mixing parameters, via the NC and CC energy spectra, will require accurate measurements of the energy of the detected particles. Again calibration is crucial, especially because of the beam differences at the near and far detector - the far detector receives a relatively larger proportion of high energy ν's compared to the near.

3.2 The MINOS Calibration System

The near and far detectors will both be fitted with Light Injection Modules (LIMs) which will be used to pulse the wavelength shifting fibres (WLS) with blue LED light [3]. This light is detected by the phototubes, which converts the initial photons into an appreciable electrical signal.

After passing through a bank of elecronics the signal is stored as a number of ADC (Analogue to Digital Converter) counts which is related to the original light level from the blue LED. The height and width of the light pulse from the blue LED can be adjusted so that a number of ADC counts per light level can measured. This process must be carried out simultaneously for each WLS and its corresponding phototube pixel and electronics channel.

The same light is also measured by an independant monitor: a pin diode. In this way a relationship between the ADC counts measured by each phototube pixel and the ADC counts measured by the pin diode can be found. This allows a direct comparison between the responses of all the tubes. (The responses from each tube cannot be compared directly as different pixels may have different gains.)

The ultimate goal of the calibration system is to be able to relate the number of ADC counts measured by a pixel to the energy deposited by a minimum ionising particle (MIP). This can be done by studying muons that pass through the calorimeter in order to get the a relationship of the form: ADC counts per Muon Energy Unit (MEU). The benefit of this to the calibration is that muons of a particular energy will always look the same and so energy measurements in MEU's obtained at the near and far detectors can be directly compared. The calibration measurements will be performed at the near detector by looking at beam muons of a known energy. At the far detector cosmic ray muons will be used.

4 The MINOS Mini Calibration Module

4.1 A Description of the Mini Module

The MINOS mini calibration module was designed to be as similar as possible to the real detectors in terms of the calorimeter materials and relevant dimensions. Inch thick plates of steel, which stand vertically from a base plate of steel, sandwich the active layer of solid scintillator, which is mounted to the steel frame attached to a thin 0.2cm sheet of aluminium. Green wavelength shifting fibre (WLS) embedded in the scintillator is used to transport the light out of the calorimeter module.

The mini module consists of 16 planes in total and the steel cross-section measures $\sim$21 x $\sim$17 cm. Each scintillator layer consists of four strips, each strip having width 4.1cm, thickness 1.0cm and length 20cm. Alternate scintillator layers are offset from each other by 1.0cm along the direction of their width. Figure 4 shows a photograph of the mini module.

The entire module is fixed in an aluminium box which has been designed to accommodate two end readout from each scintillator strip via the WLS. It has also been fitted with a light injection system, which allows each WLS to be pulsed with blue light from an ultra bright LED. Light from the LED is transported via clear optical fibre to one of a number of specially designed boxes, through which the WLS is fed. The design allows as much light as possible to be transmitted from the clear

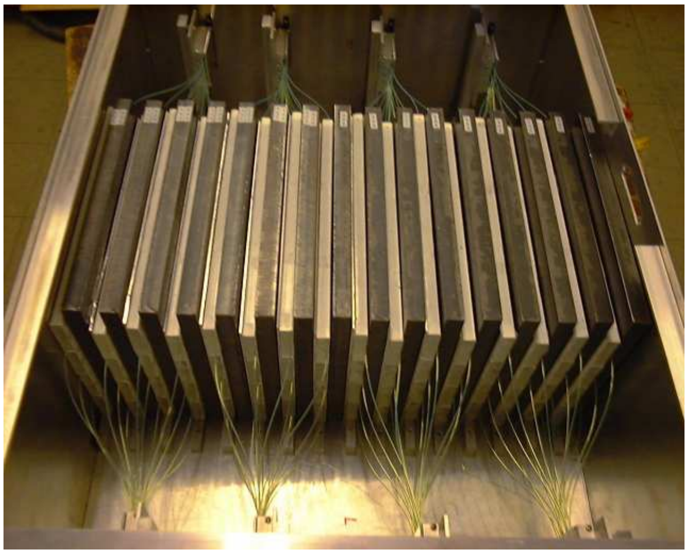

Figure 4: A photograph showing the steel and scintillator planes of the mini calibration module

fibre to the WLS, thus allowing artificial signals to take the same route as signals resulting from the passage of a particle through the calorimeter.

At the sides of the aluminium box surrounding the calorimeter, specially machined optical connectors have been used to facilitate the transmission of light from the WLS to clear fibres which then allow the photons to complete their journey to the photodetectors. The light from the module is read out from one side by four Hamamatsu M16 photomultiplier tubes, each having 16 pixels, and on the other by a Hamamatsu M64 phototube which has 64 pixels. The signals are preamplified before being read out by CAMAC analogue to digital converters (ADC's).

4.2 Understanding the Signals

As described in section (3.2), an important part of calibration is the determination of a value of ADC counts for each pixel of each phototube that corresponds to the passage of a particle with a well known amount of energy deposition. In order to carry this out, it is essential to have a good understanding of the workings of the phototubes. If a set of universal variables, common to all phototube pixels can be measured then direct comparisons between lights yields from each scintillator strip can be made. However, due to the highly statistical nature of phototubes, this process is complicated and requires correspondingly high statistics to make measurements.

A photomultiplier tube consists of a photocathode, a series of dynodes and an anode. For low numbers of photons incident at the photocathode, one may expect that the probability of getting 0,1,2,3... photons follows a poisson distribution. The quantum efficiency of the photocathode gives the probability that an incident photon will cause the emission of a photoelectron, but this is just a number and so one would also expect that the probability of getting 0,1,2,3... photoelectrons also follows a poisson distribution.

As these initial photoelectrons hit the first dynode, it has been shown that the number of secondary particles emitted also follows a poisson distribution (separately for each of the initial photoelectrons). This is also true at each successive dynode. At the end of such a cascade, the total charge is collected at the anode.

Despite the large range of signals that an initial number of photoelectrons can seemingly result in, a large number of measurements of a particular low light level (where poisson statistics apply to the photon distribution) produce a spectrum in which the signals due to an initial single photoelectron can clearly be distinguished as a peak. In some cases, at higher PMT voltages the 2 photoelectron peak can also be identified.

Due to the fact that poisson statistics govern the initial photon and photoelectron distributions, the spectra can be used to calculate the mean number of initial photoelectrons produced from the cathode for a particular light level. Given that the number of photoelectrons is directly related to the number of original incident photons by the quantum efficieny (which we can consider a constant for a particular type of tube), it is fair to say that a calculation of the number of photoelectrons is a good universal variable which can be used to compare the light yields from different scintillator strips.

Another important feature of the spectrum is the existance of a pedestal. Random fluctuations in the PMT and amplifiers, when there is no light, results in small amounts of current being detected by the ADCs. This causes a 'zero' measurement of light to have a finite width. To prevent these pedestal readings from being confused with real signals, the ADC zero value is offset such that the full width of the pedestal can be seen.

The pedestal appears in the spectrum as a narrow gaussian distribution, and its area essentially measures the number of times that no photoelectrons were produced at the photocathode. Accurate measurements of the pedestal can be made by sampling the PMT signals when no light is present. By knowing the mean and variance of the pedestal, its effect can be accounted for in a spectrum for which the light level is non-zero.

Figure 5 is an example of a typical spectrum.

This model of the PMTs was used to develop a fitting program which returns, among other variables, a value for the mean number of photoelectrons. However, the program is very sensitive to the starting parameters and so performing a large number of fits, as is necessary for this report, would be very time consuming. A

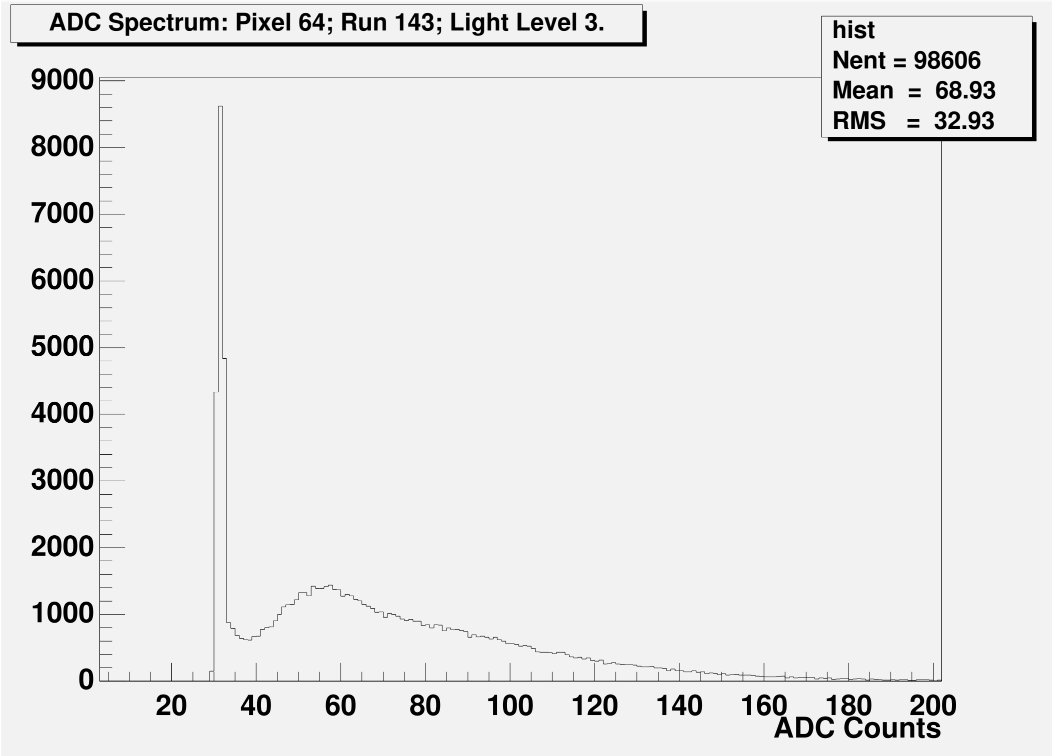

Figure 5: A typical spectrum obtained after many events taken at a single light level.

number of other approximations for the mean number of photoelectrons can also be derived using the fact that the original distribution is poisson. A particularly useful one is:

$$mean\ number\ of\ photoelectrons\ \approx \mu^2/\sigma^2$$

where $\mu = mean\ of\ the\ spectrum\ -\ mean\ of\ the\ pedestal\ peak$
and $\sigma^2 = (width\ of\ the\ spectrum)^2\ -\ (width\ of\ the\ pedestal\ )^2$

4.3 The CERN Test Beam

To test the mini module, beam time was booked at the Proton Synchrotron at CERN. The energy of the beam is 3.5 GeV and it consists of pions. The particles are directed to the beam area during two ~0.5 second spills within a ~12 second cycle.

Between spills, the opportunity was taken to use the light injection system and to take pedestal data. This was ideal in that each set of beam data would have a corresponding set of LED pulser data with which each phototube pixel could be calibrated.

Triggering on a certain type of beam event was acheived with the combination of scintillation counters and electronic logic. The LED pulser events were triggered using the same signal that tells the LED to pulse. Data acquisition was carried out using CAMAC hardware and specially written software.

5 Preliminary Calculation of the MIP Point for the MINOS Mini Calibration Module

The MIP point, for this experiment, is a single number which represents the light production of the mini module. It quantifies the amount of light produced on average in a scintillator strip when a minimum ionising particle passes through it. The MIP point is expressed in terms of a mean number of photoelectrons produced at a photocathode.

5.1 Fitting the LED pulser data

The measurement of the MIP point for the mini module is made using run 143 from the test beam data. At this time, the M64 phototube was unavailable and so data was only collected from one side of the module using the four M16 phototubes. During the run, 6 different settings were used for the LED corresponding to 6 different light levels which were used for the calibration. (For simplicity, level 1 will be used to refer to the lowest light level and level 6 to the highest.) For each setting ~99000 events were taken as well as ~143000 pedestal events.

Beam events were triggered by demanding that signals were received in coincidence from scintillation counters at the front and back of the calorimeter. Therefore only events that appeared to have particles passing through the whole length of the detector were read out. With this set-up, 3151 beam events were recorded.

The first part of the analysis involves producing a calibration plot for each phototube pixel relating number of photoelectrons to number of ADC counts. One would expect that this is a straight line passing through the origin. To calculate the coefficients of the line, the 6 sets of LED pulser data for each pixel would ideally be fitted using the fitting program mentioned in section (4.2). Unfortunately, due to time constraints, it would not have been possible to perform the necessary 384 fits, and so the $(mean/sigma)^2$ method was used instead. The number of photoelectrons can then be plotted against the mean number of ADC counts from the spectrum (the mean from the corresponding pixel's pedestal spectrum having been subtracted).

A number of the resulting calibration plots with the fitted straight line are shown in figure 6.

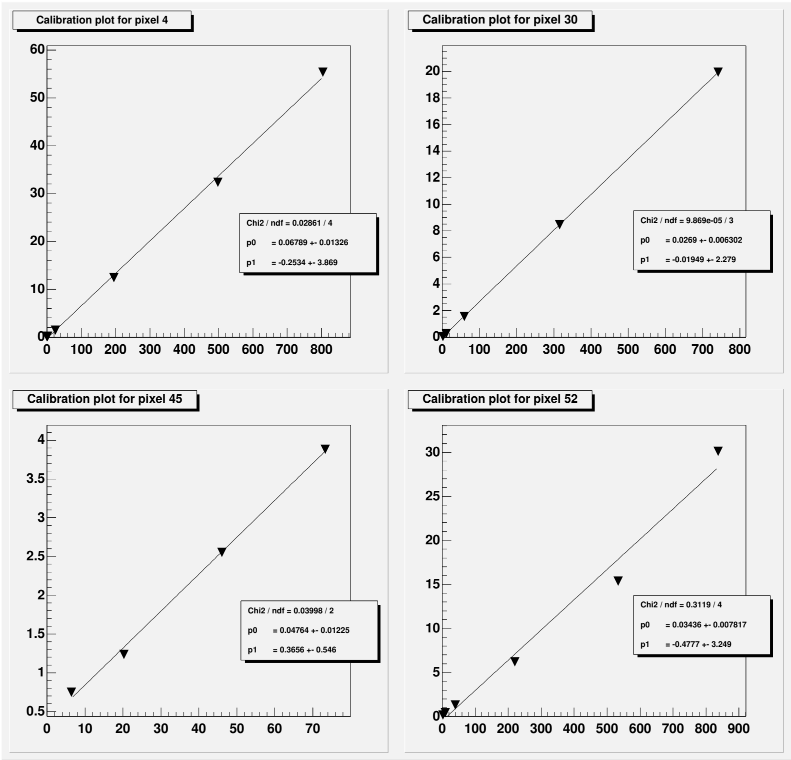

Figure 6: Calibration plots

At higher light levels, some of the ADC channels become saturated. The spectra resulting from this are characterised by having a high mean but small width. These spectra cannot be used in the calibration as they no longer scale with the amount of light detected by the phototube and so these points must be identified and discarded before the straight line fit is performed. Saturation can result for a number of reasons, for example, a high gain value in a phototube pixel or a high pedestal value, (or a combination of the two).

5.2 MIP Selection and ROOT Event Display

An interactive program for displaying 2-D and 3-D views of individual events was developed in C(++) for use in the ROOT data analysis environment. The program allows the user to view the relative amounts of light detected by individual scintillator strips as well as the development of showers through the calorimeter. The display was originally written to show simulated events generated by Geant (section (5.3)) but has been adapted to display test beam events.

Another adaption allows certain types of events to be selected and displayed. For example, a showering event, either hadronic (due to the pions) or electromagnetic (due to a small fraction of electrons also in the beam) is selected by demanding that at least 3 consecutive planes contain at least 3 scintillator strips that have seen light. The threshold for 'seeing light' is expressed in terms of photoelectrons: less than 1/3 of a photoelectron is a reasonable cut. If the threshold was much higher than this then a significant proportion of the one photoelectron events would be rejected. This cut has been adopted for the whole analysis.

For the calculation of number of photoelectrons per MIP, a set of cuts were chosen to select muon events. A track based cut was used to look for events which passed through one of seven possible paths parallel to the beam direction. Only the first 8 planes were used for this selection - demanding a higher number may have caused muons entering the detector at an angle to the beam line to be rejected.

Also, at least 11 planes with only one hit strip were required for selection. This cut is necessary on top of the track cut to ensure that the track is in fact due to a MIP, and not just a series of small showers which happen to deposit energy along one of the paths. It was also checked that no more than two planes had greater than two hit strips, thus eliminating the chance that the event would also pass the cuts for a showering event.

Muon events were expected to be present due to pion decay in the beam. A possible background to the muons are pions which don't undergo strong interactions immediately. In this case, it is possible for a pion to penetrate a number of planes only undergoing coulomb scattering and therefore will look like a MIP in the detector up until the point it showers. It is necessary to reject these events to prevent large energy depositions from the showers from being included in the calculation for the MIP point. The efficiencies of these cuts were checked using GEANT simulations (section (5.3)).

Figure 7 shows one of the selected events, upon which, the seven allowed tracks have been superimposed.

5.3 Comparison with GEANT Simulation

A Fortran program calling GEANT subroutines was adapted in order to simulate events in the mini module. The detector geometry was coded and 10,000 events were simmulated for 3.5 GeV muons and pions. The selection criteria were used to select MIP energy deposits from the generated events. The energy deposited per strip in MeV was calculated by GEANT and these values were translated into an initial number of photoelectrons at the photocathode.

The selection program rejected 0.52% of the muon events and accepted 0.0% of the pion events. These figures indicate that events passing the cuts are likely to constitute a very pure sample of muons.

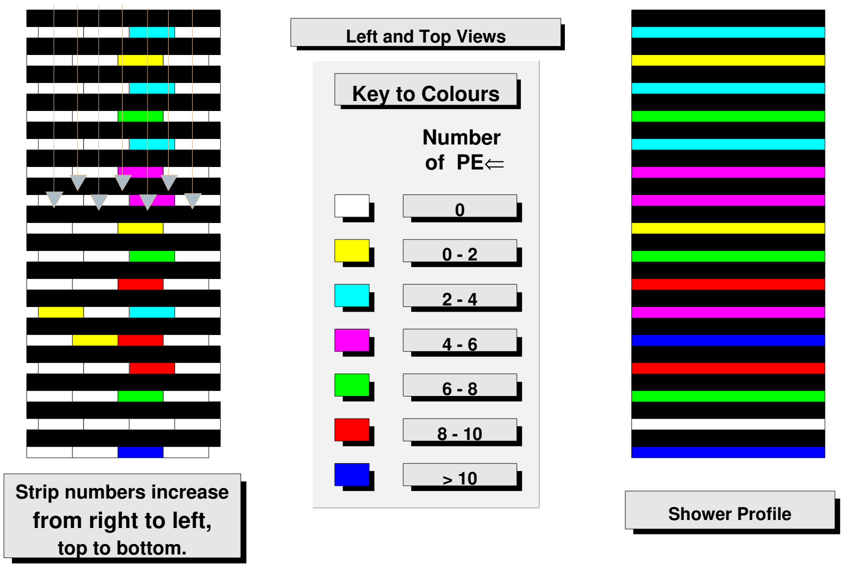

Figure 7: Display showing one of the selected MIP events. The beam enters at the top of the display and the squares represent scintillator strips. The arrows show the possible tracks accepted by the event selector.

5.4 Calculating the MIP Point

The calibration plots were used to calculate the ADC counts threshold corresponding to 1/3 of a photoelectron for each phototube pixel, and MIP events were selected from the beam data. The events which passed the cuts were then used to calculate a mean number of photoelectrons corresponding to the passage of a MIP through a scintillator strip. The number of photoelectrons measured in the strips that participated in the tracks were histogrammed.

For run 143, 1.3% of the events passed the cuts. The number of photoelectrons in each of the strips in the track were histogrammed as well as in strips from any of the other eight planes for which only one strip was hit. This resulted in 562 individual measurements of the MIP energy in a scintillator strip.

The Landau distribution describes the energy loss by a particle passing through thin strips of material and is characterised by having a high peak and long tail. Evidence of this behaviour is visible in the histogram produced (figure 8). However, relationship between ADC counts and number of photoelectrons, calculated from the calibration plots, is only an average value and in reality there is still a spread of ADC values for each photoelectron emitted from the photocathode. This is reflected in the imperfect fit to the data also shown in figure 8.

A perhaps more useful fit is a gaussian distribution fitted only to the peak in the histogram. This gives information about the energy typically deposited by a MIP passing through a scintillator strip. The fit is shown in figure 8. From this fit, a preliminary value for the MIP point was found to be 3.6 ± 0.1 photoelectrons.

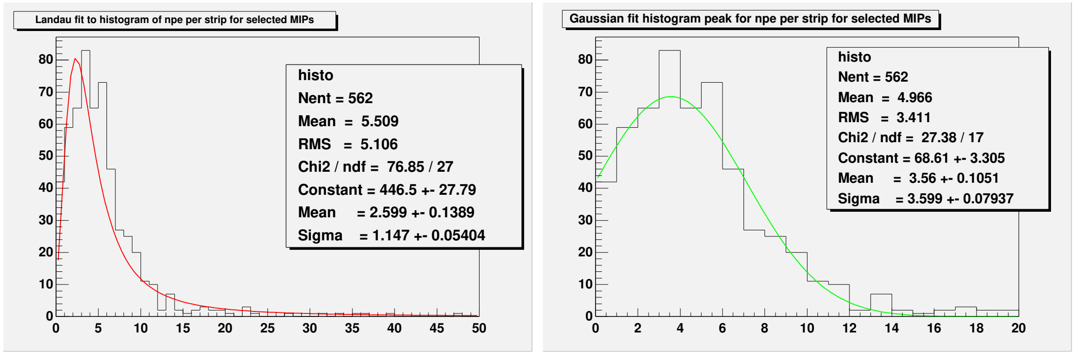

Figure 8: left: A histogram of energy deposited per scintillator strip, used to calculate a value for the MIP point. A Landau dstribution has been fit to the data; right: The peak from the same histogram with a gaussian fit.

6 Conclusions

The preliminary value of 3.6 photoelectrons per MIP per scintillator strip gives an indication of the light production of the mini calibration module. The number is encouraging in that it is well above the 0.33 cut-off to distinguish against pedestal events. Ideally, of course, the more photoelectrons the better as this allows greater sensitivity to smaller energy deposits. For this reason, it is advantageous to ensure that as little light as possible is being lost from the system. Problems potentially causing a loss include crazed optical fibres, bad optical connectors or inferior scintillator. However, it is necessary to repeat the MIP point calculation before any conclusions about light loss from the mini module can be made.

The next stage would be to use the MIP point to convert all other events detected in the module into muon energy units, in order to understand typical characteristics of different types of particle showers in the calormeter. This would also provide an independant check that the MIP point is reasonable, by comparing total energy deposits with GEANT simulations.

A more accurate value for the MIP point can be calculated by considering a number of changes to the procedure outlined in this report. Firstly, rather than using the $(mean/sigma)^2$ method to approximate the number of photoelectrons, the fitting program mentioned in section (4.2) could be employed.

A more intelligent track-finding selection program, able to find tracks that deviate slightly from a straight path is also preferable. Then only the the hit strips in the track need be histogrammed which would prevent signals due to noisy channels, or other random particle hits, from being included without having to reject any real signals, (as has been done in this project).

Finally, more statistics are necessary to fully define the shape of the MIP photoelectron spectrum. The final shape will be a convolution of a Landau distribution and some PMT function. However, with enough statistics the main peak is likely to be more defined and will give an indication of the the average and typical range of values for the energy deposited by a MIP in terms of photoelectrons.

7 References

1. B. Pontecorvo, JETP **33**, 549 (1957); JETP **34**, 247 (1958); Zh. Eksp. Teor. Fiz. **33**, 1717 (1967).

2. The MINOS Detectors Technical Design Report, FNAL Report October 1998

3. Ultra bright LED light injection calibration system for MINOS, NIM-A423(1999) 320-327, J.Thomas et al.